MODELING OF PERMEABILITY OF POROUS MEDIA WITH MIXED WETTABILITIES BASED ON NONCIRCULAR CAPILLARIES

*Junichiro TAKEUCHI[1], Hidetaka TSUJI[1] and Masayuki FUJIHARA[1]

[1]Graduate School of Agriculture, Kyoto University, Japan

*Corresponding Author, Received: 16 June 2016,   Revised: 15 Sept. 2016, Accepted: 30 Nov. 2016

ABSTRACT: Hydraulic conductivity of hydrophobic porous media is greater than that of hydrophilic porous media under the same saturation condition. One of the reasons for this is that the size of the pores filled by water in hydrophobic porous media is greater than that in hydrophilic media under unsaturated conditions. The validity of this phenomenon was ascertained through numerical experiments using a pore-network model. However, the pore-network model with circular tubes could not account for the phenomena sufficiently. Then, noncircular tubes are employed to take air-water interfaces formed at gaps between grains into account. In one case of hydrophobic grains, water cannot occupy corners and flows in the center of capillary tubes. In the other case of hydrophilic grains, water invades the corners first and flows through the corner filaments until water enters the tube completely. In this study, equilateral triangular and cuspate cross-sections are used, and the relation between the flow resistance of the tube, which is separated into shape and scale factors, and capillary pressure is investigated. The computed results show that the flow resistance of center flows could become smaller than that of full flow and that it leads to higher hydraulic conductivity of hydrophobic porous media.

Keywords: Network Flow, Variational Principle, Wettability, Air-water Interface, Hydraulic Conductance

1. INTRODUCTION

To alter hydraulic properties, such as permeability, and the water retention property of porous media, mixing grains with different wettabilities is considered to be an effective option. In particular, it is known that hydrophobic grains change hydraulic properties drastically, depending on the mixture proportion [1], [2].

Many works have attempted to model the mechanisms of imbibition and drainage inside porous media on a pore-scale [3], [4]. A pore-network model, which was first proposed by Fatt (1956) [5], is a powerful tool to model and understand the mechanisms in a bottom-up manner. In this study, the pore-network model is employed to reproduce an interesting phenomenon wherein the permeability of hydrophobic porous media becomes larger than that of hydrophilic media at the same saturation level [6]. To deal with this, the hydraulic conductance, which is a physical property assigned to each capillary tube and defined as the inverse of flow resistance in a capillary tube, needs to be reconsidered. The hydraulic conductance depends on the cross-sectional size and shape of the capillary tube and is a different property from the hydraulic conductivity, which is a macroscopic property of porous media. In this study, air-water interfaces formed between grains are considered by using noncircular capillary tubes, and hydraulic conductance is computed by solving a 2-dimensional Poisson equation whose unknown variable is the velocity in a cross-section [7]–[9].

Thus far, hydraulic conductance has had various definitions. In some definitions, pipe length and/or viscosity are included [7]–[9]. If local losses, such as contraction and enlargement in a network flow are not negligible, the pipe length needs to be included in the hydraulic conductance. However, these local losses are negligible compared with the friction loss [6]. Hence, it is natural to define the hydraulic conductance without pipe length and viscosity to correspond to the intrinsic permeability of porous media. In addition, a new method to separate the hydraulic conductance into shape and scale factors is proposed because the effect of cross-sectional shape on the flow resistance is not clear in the conventional method; in the conventional method, the Manson–Morrow shape factor (defined as area/square of wetted perimeter) is used as a shape factor [6], [7]. However, the Darcy–Weisbach friction factor also depends on the cross-sectional shape.

In this study, the shape factor and its effect on the permeability of porous media are inspected through numerical experiments, and it is shown that air-water interfaces in capillary tubes play a large role in permeability.

2. NETWORK FLOW IN POROUS MEDIA
2.1 Variational Principle in Network Flow

In general, to solve a network flow problem, the Hardy–Cross method is used. In this method, the flow rate in each pipe and potential at each junction are unknown variables, and a non-linear simultaneous equation for both the energy loss and mass conservation is formulated [10]. In this study, a method based on a variational principle is employed. The variational principle is a fundamental concept to determine a solution to some physical problems. It is based on the idea that many physical phenomena obey the basic principle that the state of the system is determined by minimizing energy consumption. In a pore-network flow problem, a functional ϕ, which is to be minimized, is defined as the summation of three terms, as follows [11]:

$$\phi(\boldsymbol{q}) = \phi^{\mathrm{F}}(\boldsymbol{q}) + \phi^{\mathrm{OUT}}(\boldsymbol{q}) + \phi^{\mathrm{IN}}(\boldsymbol{q}) \qquad (1)$$

where $\boldsymbol{q}$ is the flow rate vector whose components q_i ($i = 1,...,N^{\mathrm{tube}}$) are the flow rates in the i th capillary tube; ϕ^{F} is the friction term; ϕ^{OUT} and ϕ^{IN} are the outflow and inflow terms, respectively. The friction term is represented as follows, based on the Darcy–Weisbach equation:

$$\phi^{\mathrm{F}} = \sum_{i=1}^{N^{\mathrm{tube}}} \frac{1}{3} \kappa_i |q_i| q_i^2 \qquad (2)$$

with

$$\kappa_i = \frac{f_i l_i}{2 g d_i a_i^2}, \qquad (3)$$

$$d_i = \frac{4 a_i}{p_i} \qquad (4)$$

where N^{tube} is the number of capillary tubes included in the pore-network; κ_i is a coefficient for the friction loss; f_i is the Darcy-Weisbach friction factor; l_i , a_i , d_i , and p_i are the length, the cross-sectional area, hydraulic diameter, and the wetted perimeter of the i th capillary tube, respectively; and g is the gravitational acceleration. Here, only a friction loss is taken into account, based on the fact that other local losses, such as contraction and enlargement, are negligible compared with the friction loss [6]. When the flow in capillary tubes is laminar, the friction factor f_i is represented as follows:

$$f_i = \alpha_i / \mathrm{Re}_i \qquad (5)$$

with

$$\mathrm{Re}_i = \frac{d_i |q_i|}{v a_i}, \qquad (6)$$

$$v = \frac{\mu}{\rho} \qquad (7)$$

where α_i is a coefficient that depends on the cross-sectional shape, and the values for circular, square, and equilateral triangular sections are 64,

56.908, and 53.333, respectively [12]; Re_i is the Reynolds number; v is the kinematic viscosity; μ is the viscosity; and ρ is the water density.

The second and third terms on the right hand side of Eq. (1) are represented as follows:

$$\phi^{\mathrm{OUT}} = \sum_{i \in \zeta^{\mathrm{OUT}}} h_i q_i \qquad (8)$$

$$\phi^{\mathrm{IN}} = -\sum_{i \in \zeta^{\mathrm{IN}}} h_i q_i \qquad (9)$$

where ζ^{OUT} and ζ^{IN} are the sets of capillary tubes connected to the outflow and inflow ports, respectively; and h_i are the piezometric heads at the outflow and inflow ports, which are the prescribed variables in this study.

In addition to the functional Eq. (1), the following mass balance equations at each junction are added as constraints:

$$\sum_{k \in \zeta_j^{\mathrm{junc}}} q_k = 0 \qquad \left(j = 1,...,N^{\mathrm{junc}} \right) \qquad (10)$$

where N^{junc} is the number of junctions, and ζ_j^{junc} is the set of capillary tubes connected to the j th junction.

The minimization problem of the functional Eq. (1) with the constraints (10) is solved by the Lagrange multiplier method, which introduces Lagrange multipliers λ_j ($j = 1,...,N^{\mathrm{junc}}$). The objective problem is reformulated as a minimization problem with unknown variables $\boldsymbol{q}$ and $\boldsymbol{\lambda}$ by adding the constraints multiplied by λ_j to the functional Eq. (1).

$$\Phi(\boldsymbol{q}, \boldsymbol{\lambda}) = \phi(\boldsymbol{q}) + \sum_{j=1}^{N^{\mathrm{junc}}} \lambda_j \left(\sum_{k \in \zeta_j^{\mathrm{junc}}} q_k \right) \qquad (11)$$

where $\boldsymbol{\lambda}$ is a vector with component λ_j ($j = 1,...,N^{\mathrm{junc}}$).

Incidentally, the nonlinear simultaneous equation obtained after partial differentiation of the functional Eq. (11) by each unknown variable is exactly the same as the equation system of an ordinal network flow problem; in this problem, the flow rate in each pipe and piezometric head at each junction are unknown variables. For example, the partial differentiation of the functional Eq. (11) with respect to an unknown flow rate q_i is as follows, if the i th capillary tube connects to neither the outflow nor the inflow port:

$$\lambda_{j1} - \lambda_{j0} = \kappa_i |q_i| q_i \qquad (12)$$

where the subscripts $j0$ and $j1$ are the junction indices of both ends of the i th capillary tubes; Eq. (12) shows the local head loss by friction, which means that the Lagrange multiplier λ_j is the piezometric head at each junction. By substituting Eqs. (3)–(7) into Eq. (12), the following equation is derived:

$$q_i = \frac{\Theta_i}{\mu} \frac{\Box p_i}{l_i} \qquad (13)$$

with

$$\Box p_i = \rho g (h_{j1} - h_{j0}), \qquad (14)$$

$$\Theta_i = \frac{32 a_i^3}{\alpha_i p_i^2} \qquad (15)$$

where Θ_i is the hydraulic conductance, and $\Box p_i$ is the piezometric potential difference between junctions $j0$ and $j1$. With regard to the hydraulic conductance Θ_i, the viscosity μ and/or the tube length l_i are excluded in this study because it is natural to consider that the hydraulic conductance of capillary tubes corresponds to the intrinsic permeability of porous media.

2.2 Shape and Scale Factors

The hydraulic conductance Θ in Eq. (13) is considered to be the inverse of the flow resistance of a capillary tube and includes shape and scale factors. In previous studies, the Manson–Morrow shape factor G ($= a / p^2$) was introduced, and the hydraulic conductance was rearranged as follows [9]:

$$\Theta = 32 a^2 G / \alpha \qquad (16)$$

However, the coefficient α is also dependent on the cross-sectional shape. Then, the effective radius r_e and a coefficient β, which satisfy the following relations, are introduced here to separate shape and scale factors completely:

$$a = \pi r_e^2 \qquad (17)$$

$$p = \beta r_e \qquad (18)$$

Hence, the hydraulic conductance is represented as follows:

$$\Theta = \pi^2 r_e^4 / \eta \qquad (19)$$

with

$$\eta = \frac{\alpha \beta^2}{32 \pi} \qquad (20)$$

where η is the shape factor, which is the flow resistance of the capillary tube and depends only on the cross-sectional shape. Moreover, the coefficient β ranges from zero to infinity mathematically, which means the hydraulic conductance also could change from zero to infinity.
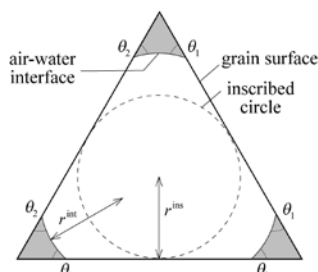
Before solving the network flow problem presented in Eq. (11), values for the shape factor η of various cross-sectional shapes needed to be specified. These are calculated from the flow rate q, based on Eqs. (13), (19), and (20). The flow rate in a constant pipe is calculated from the velocity distribution in the cross-section, and the velocity is governed by the 2-D Poisson equation; this is a simplified form of the Navier–Stokes equation and the mass conservation equation, based on the following assumptions: (1) flow is steady, (2) fluid is viscous, (3) inertia is negligible, and (4) velocity components, except for those along the tube axis, are negligible [9]. The induced Poisson equation and boundary conditions are described as follows:

$$\nabla^2 v_X = \frac{\rho g}{\mu} \frac{dh}{dX} (= \text{constant}) \qquad (21)$$

$$v_X = 0 \quad \text{on the grain-water interface} \qquad (22)$$

$$\frac{\partial v_X}{\partial n} = 0 \text{ on the grain-water interface} \qquad (23)$$

where X, Y, and Z are the local Cartesian coordinates, and X is in the direction of the tube axis; ∇^2 ($= \partial^2 / \partial Y^2 + \partial^2 / \partial Z^2$) is the differential operator; v_X is the velocity component along the X axis; and n is the unit normal vector to the interface (boundary).

When a capillary tube consists of hydrophilic grains, water tends to occupy the corners first; hence, water flows along the corner filaments as illustrated in Fig. 1. In contrast, when a tube consists of hydrophobic grains, air, which is wetting the fluid in this case, tends to occupy the corners; hence, water flows in a center filament which is contrary to the hydrophilic case. In both cases, the curvature radius of the air-water interface r^{int} is determined from the Young–Laplace equation (24) and the capillary pressure p_c as described in Eq. (25); the three-phase contact points are determined from the contact angles of the grains θ_0, θ_1, and θ_2.

$$r^{int} = \sigma / p_c \qquad (24)$$

$$p_c = p_a - p_w \qquad (25)$$

where σ is the surface tension of water, and p_a and p_w are the air and water pressures, respectively in the vicinity of the air-water interface.

Fig. 1 Schematic of corner filament in triangular capillary tube
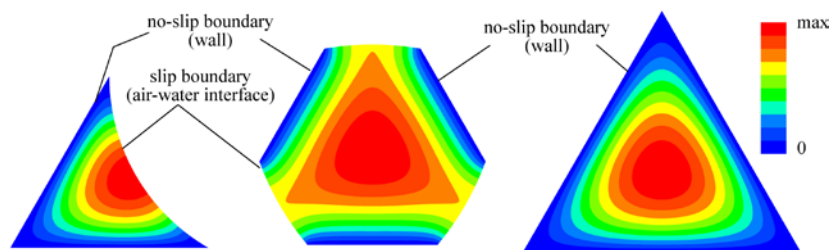
(a) Corner flow   (b) Center flow   (c) Full flow

Fig. 2 Velocity distributions in triangular capillary tube
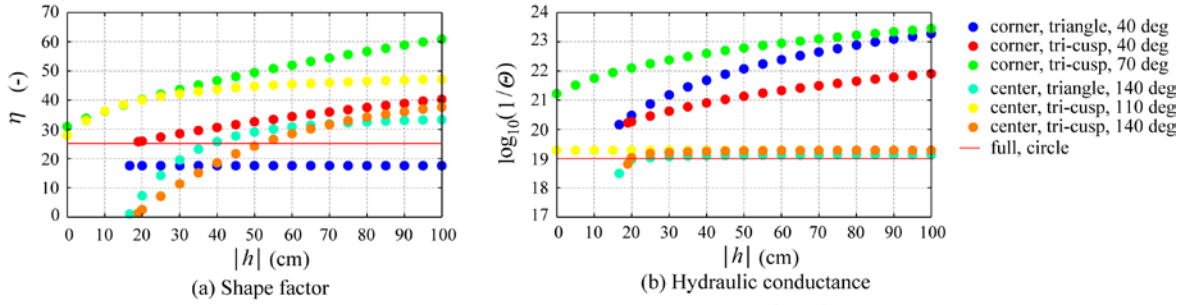
Fig. 3 Flow resistance vs. piezometric head (cross-sectional area of all tube is 1.61x10^{-3} mm^2)

In Fig. 2, some typical examples of velocity distributions obtained by solving the 2-D Poisson equation (21) in corner, center, and full flows through equilateral triangular tubes are shown; Fig. 3 shows the shape factors and hydraulic conductances of the equilateral triangular and tri-cuspate tubes as the capillary pressure varies. It is assumed that these two types of tubes have the same cross-sectional area. Fig. 3 (a) shows that cross-sections with air-water interfaces could have smaller shape factors compared with the circular tube in some ranges. Nevertheless, it is found from Fig. 3 (b) that corner filaments have a much greater flow resistance because their flow cross-sectional areas are very small compared with the whole cross- sectional area of the tube and that only center flows could have smaller flow resistances.

2.3 Hydraulic Conductivity

Hydraulic conductivity of a pore-network model is estimated based on the Darcy law:

$$K = \frac{QL}{A\Delta H} \tag{26}$$

with

$$Q = \sum_{i=1}^{N^{\text{OUT}}} q_i^{\text{OUT}} = \sum_{i=1}^{N^{\text{IN}}} q_i^{\text{IN}} \tag{27}$$

where K is the hydraulic conductivity of a variously saturated porous medium, Q is the total flow through the porous medium, A is the cross-sectional area of the porous media, and ΔH is the piezometric head difference between the inflow and outflow faces. When the porous medium is completely saturated, the hydraulic conductivity is referred to as the saturated hydraulic conductivity and represented as K_s. The relative permeability k_r is defined as

$$k_r = K / K_s \tag{28}$$

3. NUMERICAL EXPERIMENTS
3.1 Generation of Pore-network

A virtual pore-network is generated from a porous medium model that consists of randomly packed spherical grains of uniform size. The virtual porous medium is computed by the discrete element method with grains falling freely (Fig. 4 (a)), and a pore-network is extracted from the computed porous medium with the modified Delaunay tessellation method proposed by Al-Raoush et al. [13] (Fig. 4 (b)). The pore-network is composed of pore bodies that are relatively large voids and pore throats that are relatively small voids connecting two pore bodies. In Fig. 4 (b), pore bodies are represented as spheres and pore throats as tubes. The location and size of all pore bodies and throats, as well as those of grains, are

(a) Randomly packed grains

(b) Pore network model (pore body and pore throat type)

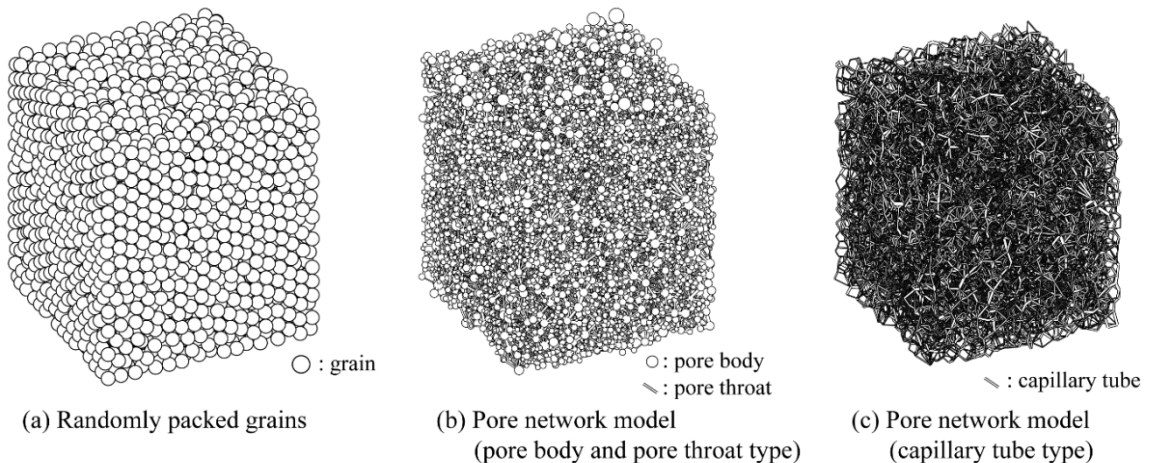(c) Pore network model (capillary tube type)

Fig. 4 Virtual porous medium and pore-network models

obtained through the generation process. In this study, the sizes of the pore body and pore throat are defined as the radius of the maximum inscribed sphere and circle inside the grain void, respectively.

3.2 Generation of Variously Saturated Pore-network

Prior to the computation of network flow problems in a porous medium, variously saturated pore-network models are generated in a generalized invasion percolation manner, which is a discrete model to simulate water or air invasion into porous media [14]. The bottom of a dry porous medium, in which pores are not occupied by water in the initial state, is supposed to be soaked in water.

The bottom and top faces of the pore-network are open-flow boundaries, and water and air pools are connected to the bottom and top faces, respectively. Moreover, the four sides are no-flow boundaries, and no fluid can pass through these boundaries. Water rises into invadable pores from the bottom if the following conditions are satisfied: (1) an objective pore is empty, and it connects to the air pool through other empty pores; (2) the objective pore connects to at least one pore that is occupied by water, and at least one of the neighboring pores occupied by water connects to the water pool through other pores occupied by water; and (3) in case of hydrophilic pores, the objective pore is sufficiently small or in the case of hydrophobic pores, the pore is sufficiently large.

Conditions (1) and (2) are referred to as connectivity conditions.

By changing the water pressure on the bottom of a pore-network, variously saturated pore-networks are obtained. In addition, hydrophobic grains are mixed at specified mixture fractions in this study. In Table 1, grain size, temperature, and the contact angles used for the imbibition process are summarized. The contact angles are those fitted with measured and computed water retention curves in our previous works [6], [14]. Fig. 5 shows examples of partially inundated hydrophilic and hydrophobic pore-networks. While water can enter hydrophilic media under negative pressure conditions, positive pressure is required for water to enter hydrophobic media by capillary action. Hence, negative and positive pressures are imposed on hydrophilic and hydrophobic media, respectively, to obtain the partially saturated pore-networks shown in Fig. 5. It is found that water invades smaller pores selectively in the hydrophilic pore-network;, conversely, water invades larger pores selectively in the hydrophobic pore-network.

3.3 Relative Permeabilities

According to our previous work [6], for the computation of network flows, the pore-network is regarded as consisting of volumeless pore bodies and pore throats with constant cross-sections. The pore-network model used for network flow problems is as shown in Fig. 4 (c).
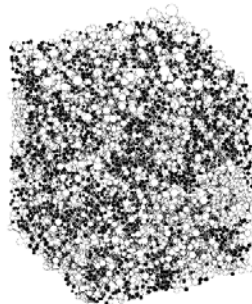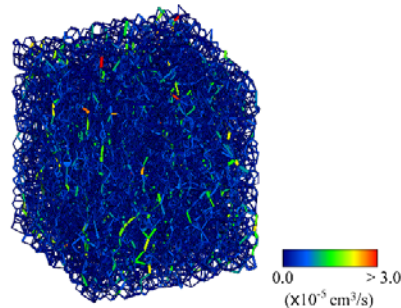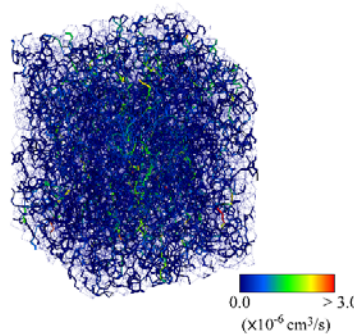

(a) hydrophilic porous medium
(-20 cmH$_2$O, 0.44)
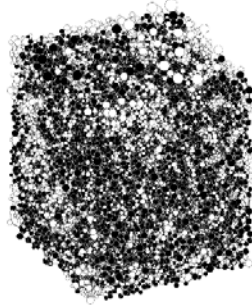
(b) hydrophobic porous medium
(20 cmH$_2$O, 0.59)

● \ : Water-filled pore   ○ \ : Air-filled pore

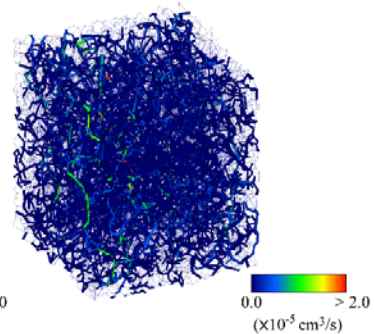Fig.5   Inundation into hydrophobic
and hydrophilic media
(piezometric head posed on bottom, saturation)

(a) fully saturated porous medium
(0 cmH$_2$O, 1.00, 2.3×10^{-2} cm/s)

(b) hydrophilic porous medium
(-20 cmH$_2$O, 0.44, 5.6×10^{-4} cm/s)

(c) hydrophobic porous medium
(20 cmH$_2$O, 0.59, 1.7×10^{-2} cm/s)

Fig.6   Flow distributions of variously saturated porous media
(piezometric head posed on bottom, saturation, hydraulic conductivity)

Table 1 Conditions for permeability test		
Grain diameter		0.2 mm
Air pressure		1 atm
Water pressure		4 cm H_2O
Temperature		20 °C
Contact angle	mixture rate: 0%	46°
	mixture rate: 25%	92°, 110°
	mixture rate: 50%	98°, 110°
	mixture rate: 75%	98°, 110°
	mixture rate: 100%	110°

Other conditions for the permeability test, such as air and water pressures, are listed in Table 1. Both the top and bottom of the pore-network is subject to water pressure, and water flows downwards under gravity in this numerical test. When the contact angle is between 60° and 120°, partial invasion, such as corner and center filaments, will not occur in the equilateral triangular tubes. Tri-cuspate tubes are used here.

In this model, only one parameter needs to be fitted. The unknown parameter is the effective radius of the capillary tubes, and it is represented as with a function of the inscribed radius r_{ins} as follows:

$$r_e = \gamma r_{ins} \tag{29}$$

where γ is the unknown parameter. The value is adjusted by comparing measured and computed hydraulic conductivity in a fully saturated state, where there are no air-water interfaces. In this study, the unknown parameter γ is adjusted so that the saturated conductivity is approximately 2×10^{-2} cm/s. When γ is 1.11, the saturated hydraulic conductivity is 2.3×10^{-2} cm/s.

Network flow problems regarding the variously saturated pore-networks are solved, and the relative permeability of each pore-network is calculated. In Fig. 6, typical flow distributions of completely and partially saturated cases are shown. These figures show that water flow is limited to only some parts of the capillary tubes and that the majority of tubes do not contribute to water flow. In Fig. 7, measured and computed relative

permeabilities are shown. The measured value was obtained using the constant water-level method with samples containing various ratios of mixed hydrophilic and hydrophobic glass beads. Samples were variously saturated by sucking air with different suction forces after dipping their bottoms into water. Thus, all hydrophilic samples (0% in Fig. 7 (a)) became highly saturated. In the computed result (Fig. 7(c)), full flow was applied in the samples with saturation levels over 0.95 because the air-water interfaces were considered to have developed poorly. From the computed result (Fig. 7 (b)), it is found that the relative permeabilities of hydrophobic media (25–100%) are larger than those of the hydrophilic (0%). This is because water enters the larger pores first in hydrophobic media, as shown in Fig. 5. In addition to this pore size effect, compared with the computed results (Fig. 7 (b) and (c)), the relative permeabilities of hydrophobic media with tri-cuspate tubes are larger than those with circular tubes, which is the effect of the air-water interfaces. Although there is some discrepancy in the low saturation region between the measured and computed results, the phenomenon involving the permeability of hydrophobic porous media is more significant than that of hydrophilic media at the same saturation and is well reproduced by using tri-cuspate tubes.

4. CONCLUSION

In this study, noncircular tubes were employed in a network flow modeling of porous media to take air-water interfaces formed between grain gaps into consideration. The network flow problem is formulated with a variational principle. From the numerical analysis of the hydraulic conductance of the tube cross-section, it was shown that the flow resistance of cross-sections with air-water interfaces, which are slip boundaries for water flow, could be smaller than that in full flow under a low pressure condition. Moreover, through numerical experiments, it was ascertained that not only the tube size, but also the air-water interface,
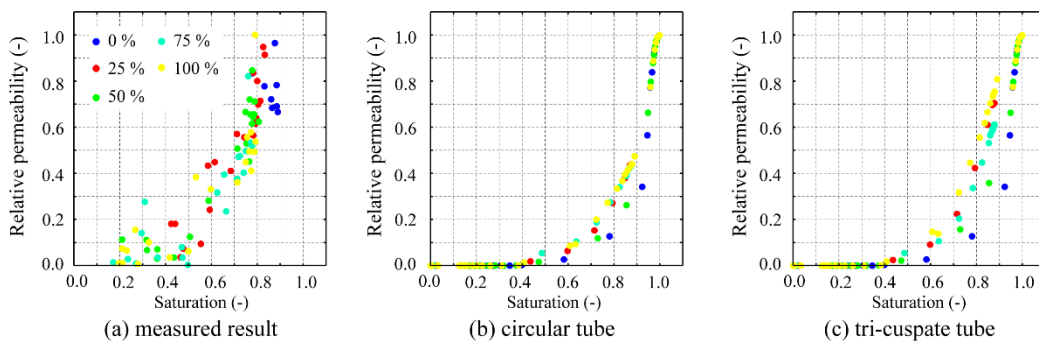

Fig. 7 Measured and computed relative permeability

contributes to the increase in permeability of unsaturated hydrophobic porous media.

5. REFERENCES

[1] DeBano LF, "Water repellency in soils: a historical overview", J. Hydrol., Vol. 231-232, 2000, pp. 4-32.

[2] Annaka T, "Wettability indices and water characteristics for sands of mixed wettability", J. Jpn. Soc. Soil Phys., Vol. 102, 2006, pp. 79-86 (in Japanese).

[3] Ustohal P, Dtauffer F, and Dracos T, "Measurement and modeling of hydraulic characteristics of unsaturated porous media with mixed wettabilities", J. Contam. Hydrol., Vol.33, 1998, pp. 5-37.

[4] Takeuchi J, Takahashi T., and Fujihara M, "Sub-Darcy scale modeling of non-uniform flow through porous media with mixed wettabilities", Int. J. GEOMATE, Vol. 6, 2014, pp. 840-847.

[5] Fatt I, "The network model of porous media", Trans. AIME, Vol. 207, 1956, pp. 144-181.

[6] Takeuchi J, Sumii W, Tsuji H, and Fujihara M, "Estimation of permeability of porous media with mixed wettabilities using pore-network model", Int. J. GEOMATE, Vol. 11, 2016, pp. 2241-2247.

[7] Blunt MJ, Jackson MD, Piri M, and Valvatne PH, "Detailed physics, predictive capabilities and macroscopic consequences for pore-network models of multiphase flow", Adv. Water Resources, Vol. 25, 2002, pp. 1069-1089.

[8] Valvatne PH and Blunt MJ, "Predictive pore-scale modeling of two-phase flow in mixed wet media", Water Resour. Res., Vol. 40, 2004, W07406, doi: 10.1029/2003WR002627.

[9] Raoof A and Hassanizadeh SM, "A new formulation for pore-network modeling of two-phase flow", Water Resour. Res., Vol. 48, 2012, W01514, doi: 10.1029/2010WR010180.

[10] Larock BE, Jeppson RW, and Watters GZ, Hydraulics of Pipeline Systems, CRC Press, 2000, p. 537.

[11] Bando O, Flows in pipe network and pump solved with excel, Kogyo Chosakai Publishing, 2008, p. 157 (in Japanese).

[12] Shah RK, "Laminar flow friction and forced convection heat transfer in duct of arbitrary geometry", Int. J. Heat Mass Transfer, Vol. 18, 1975, pp. 849-862.

[13] Al-Raoush R, Thompson K, and Willson CS, "Comparison of network generation technique for unconsolidated porous media", Soil Sci. Soc. Am. J., Vol. 67, 2003, pp. 1687-1700.

[14] Takeuchi J, Sumii W, and Fujihara M, "Modeling of fluid intrusion into porous media with mixed wettabilities using pore-network", Int. J. GEOMATE, Vol. 10, 2016, pp. 1971-1977.